High Torque Slow Rotational Speed Permanent Magnet Synchronous Machine Technical Evaluation

Lappeenranta–Lahti University of Technology LUT

Master's Programme in Electrical Engineering, Master's Thesis

2023

Jesse Kurronen

Examiner(s): Docent, Janne Nerg

M.Sc., Otto Suuronen

ABSTRACT

Lappeenranta–Lahti University of Technology LUT

LUT School of Energy Systems

Electrical Engineering

Jesse Kurronen

High Torque Low Rotational Speed Permanent Magnet Synchronous Machine Technical Evaluation

Master's thesis

2023

54 pages, 24 figures and 13 tables

Examiner(s): Docent Janne Nerg, D.Sc. (El.Eng)

Otto Suuronen, M.Sc. (El.Eng)

Keywords: Fractional slot winding, Integer slot winding, High torque, Low rotational speed, Permanent Magnet Synchronous Machine

The objective of this thesis was to evaluate if certain low rotational speed, high torque application is feasible with permanent magnet topology. Electromagnetic performance, efficiency and material costs were compared.

Thesis gives a brief overview of high torque, low rotational speed machines, and their application areas. These machines were studied, and different possible topologies are shown. Electromagnetic and mechanical properties of different winding types were compared and types that could be manufactured as part of segmented machine structure were chosen for comparison. Comparison is made utilizing literature study, analytical calculations, and finite element analysis. Integer slot and fractional slot concentrated winding machines were analysed and compared thoroughly with different rotor topologies. Both winding types with rotor surface mounted permanent magnets were analysed. Fractional slot concentrated winding machine was shown to have more losses in permanent magnets and rotor yoke than is acceptable and for further study interior permanent magnets design with lamination stack was created. Because of interior permanent magnets design, more magnet volume and winding turns was needed to achieve the same efficiency as with integer slot wound surface mounted permanent magnet machine.

As a result of this thesis, machine design with integer slot winding and surface mounted permanent magnets was created. This machine was compared with typical electrically excited synchronous machines and found to have better efficiency and lower material cost and mass.

TIIVISTELMÄ

Lappeenrannan–Lahden teknillinen yliopisto LUT

LUT Energiatekniikka

Sähkötekniikka

Jesse Kurronen

Korkean vääntömomentin ja hitaan pyörimisnopeuden omaavan kestomagneettitahtikoneen tekninen arviointi

Sähkötekniikan diplomityö

2023

54 sivua, 24 kuvaa ja 13 taulukkoa

Tarkastaja(t): Dosentti Janne Nerg, TkT (sähkötekniikka)

Otto Suuronen, DI (sähkötekniikka)

Avainsanat: murtovakokäämitys, kokovakokäämitys, suuri vääntömomentti, hidas pyörimisnopeus, kestomagneettitahtikone

Tämän diplomityön tavoitteena oli arvioida kestomagneettitahtikoneen soveltuvuutta korkeaa vääntömomenttia ja hidasta pyörimisnopeutta vaativaan käyttökohteeseen. Sähkömagneettista suorituskykyä, hyötysuhdetta ja materiaalikustannuksia vertailtiin.

Diplomityö antaa katsauksen erilaisiin käyttökohteisiin, jotka vaativat suuren vääntömomentin ja hitaan pyörimisnopeuden omaavan sähkökoneen. Erilaisia suuren vääntömomentin tuottavia hitaasti pyöriviä sähkökoneita tutkittiin ja mahdolliset konerakenteet esitettiin. Myös erilaisia käämitystyyppejä vertailtiin ja käämitysvaihtoehdot, jotka ovat valmistettavissa segmentoituun rakenteeseen valittiin jatkotutkimuksiin. Vertailu suoritetiin tutkimalla kirjallisuutta, analyyttisillä laskelmilla sekä numeerisilla, elementtimenetelmään pohjautuvilla analyyseillä. Kokovakokäämitys sekä murtovakokäämitys tutkittiin ja vertailtiin eri roottorirakenteilla. Molemmat käämitystyypit arvioitiin pintamagneettiroottorirakenteella. Murtovakokoneen osalta kestomagneettien ja roottorin selän häviöiden huomattiin olevan yli hyväksyttävän tason. Jatkotutkimuksia varten murtovakokonetyypille laskettiin myös uppomagneetti roottorirakenne. Laskennan perusteella havaittiin, että uppomagneetti roottorirakenteesta johtuen, murtovakokone vaatii enemmän kestomagneettimateriaalia ja käämikierroksia saavuttaakseen saman hyötysuhteen, kuin kokovakokäämityksellä oleva pintamagneeteilla varustettu kone.

Diplomityön tuloksena suunniteltiin kokovakokäämitty pintamagneeteilla oleva suoravetoinen kestomagneettitahtikone. Tätä konetta vertailtiin olemassa oleviin sähköisesti magnetoituihin tahtikoneisiin ja todettiin sen saavuttavan paremman hyötysuhteen matalemmilla materiaalikustannuksilla ja massalla.

SYMBOLS AND ABBREVIATIONS

Roman characters

A	linear current density	[A/m]
B	magnetic flux density	[T]
E	electromotive force	[V]
f	frequency	[Hz]
D	diameter	[m]
d	thickness	[m]
H	magnetic field strength	[A/m]
I	current	[A]
L	inductance	[H]
j	current density	[A/mm^2]
k	coefficient,	
	factor	
l	length	[m]
m	number of phases	
N	number of winding turns	
n	rotational speed,	[rpm]
	denominator of fraction	
P	power	[W]
p	pressure,	[bar, Pa]
	number of pole pairs	
Q	number of slots	

q	number of slots per pole and phase	
r	radius	[m]
S	apparent power	[VA]
T	temperature,	[ºC, K],
	torque	[Nm]
t	time	[s]
U	voltage	[V]
V	volume	[m^3]
v	harmonic number	
w	width	[m]
y	coil pitch	[m]

Greek characters

α	relative pole width	
η	angle	[°, rad]
σ	conductivity,	[S/m],
	tangential stress	[N/m^2]
ξ	winding factor	
τ	pitch	[mm]

Constants

g	gravitational acceleration	9,81 m/s

Subscripts

add	additional loss
ag	airgap
cu	copper loss
d	d-axis
dr	rotor drum
e	excess
f	stacking
fr	friction
h	hysteresis
m	magnetizing
n	nominal
nl	no-load
PM	permanent magnet
p	pole
q	q-axis
rt	rotor
s	slot
st	stator
tan	tangential
v	voltage vector

Abbreviations

CFD	Computational Fluid Dynamics

FEA	Finite Element Analysis
FEM	Finite Element Method
FSCW	Fractional Slot Concentrated Winding
IPM	Interior Permanent Magnet
ISW	Integer Slot Winding
SPM	Surface Permanent Magnet

Table of contents

Abstract

Symbols and abbreviations

1 Introduction 10
2 High Torque Low Rotational Speed Electrical Machine 12
2.1 Physical Structure 12
2.2 Permanent Magnet Excited Versus Electrically Excited Synchronous Machines 14
3 Fractional Slot Concentrated Winding Versus Integer Slot Distributed Winding 17
3.1 Electromagnetic Comparison 17
3.1.1 Winding factor 18
3.1.2 Loss Distribution 19
3.2 Mechanical Comparison 21
4 Design and Calculation Results Comparison 25
4.1 Preliminary Simulations and Comparison 25
4.1.1 No-load Simulations and Losses 27
4.1.2 Nominal Point Simulations 33
4.2 FSCW with Interior Permanent Magnets 34
4.2.1 No-load Simulation 36
4.2.2 Nominal Point Simulation 37
4.3 Comparison of the Machine Designs 38
4.4 Design Optimization and Simulations 39
4.4.1 No-load Simulation 40
4.4.1 Nominal Point Simulation 41
4.4.2 Overload Simulation 42
4.4.1 Short Circuit Simulation and Demagnetization Evaluation 43
4.4.2 Unbalanced Magnetic Pull 50
5 Conclusions and Discussion 52
References 53

1 Introduction

Electricity consumption of electrical machines in industry is almost 40 % of the whole electricity consumption of the world (Gavrila, (Paltanea), Paltanea, Scutaru & Peter 2017). Efficient high torque, low rotational speed electrical machines have high demand in industry. Typical industries that utilize these types of special machines includes iron and steel, water management, mining, and oil and gas. Many of these industries and their applications for high torque low rotational speed synchronous machines are undergoing modernization in the future. Machines that are used in these applications are mostly electrically excited synchronous machines. (The Switch Engineering Oy 2021).

Typical electrically excited synchronous machine has reasonably long airgap because of the mechanical structure. This leads to relatively wide rotor pole and low electrical frequency due to decreased number of poles. With narrow pole width with relatively long airgap, leakage flux between rotor poles increases significantly (Kana Padinharu et al. 2020). With permanent magnets, large pole count machines are possible. This rises electrical frequency in low-speed applications and normal converters would be feasible. Permanent magnet machine requires relatively short airgap to perform effectively with reasonable amount of permanent magnet material. With preliminary understanding, this large airgap diameter machine could be manufactured to stay in specified eccentricity limit of 4mm.

The goal of this thesis is to evaluate the applicability of permanent magnet synchronous machines in a certain high torque low speed application. Permanent magnet machine topology provides more simple structure compared to electrically excited machines. Permanent magnet machines usually have higher torque density than other types of electrical machines, which leads to higher efficiency and torque production with lower mass. Decreased mass creates lower mechanical forces to the structure and aids in mechanical design. Evaluated design show feasibility of different winding topologies used in surface mounted permanent magnet machines in this low-speed high torque application.

Different winding and rotor topologies are compared utilizing literature, analytical calculations, and finite element analysis. Besides electromagnetic performance, mechanical and environmental restrictions and requirements are also considered. Mechanical restrictions and requirements include manufacturability, assembly, serviceability, and handling of the

parts. Machine thermal behaviour is not verified during this thesis, but analytical model has estimates for winding and permanent magnet temperatures.

2 High Torque Low Rotational Speed Electrical Machine

In this chapter, high torque, low rotational speed machine structures are explained. Machine sizing through torque demand and constraints is shown. Main differences between permanent magnet synchronous machines and electrically excited synchronous machines are presented and their advantages and disadvantages are discussed.

2.1 Physical Structure

High torque, low rotational speed electrical machines become large as available torque is related to rotor volume and tangential stress. Machines rough sizing can be done using previously mentioned parameters when feasible values of tangential stress for certain machine topology is known. Tangential stress σ_{Ftan} in the airgap can be expressed by following equation (1).

$$\sigma_{\mathrm{Ftan}} = \frac{1}{2}\hat{B}_{\mathrm{ag}}\hat{A}\cos\varphi, \tag{1}$$

where $\hat{B}_{\mathrm{ag}}$ is peak flux density in airgap, $\hat{A}$ is peak linear current density and $\cos\varphi$ is the power factor. Machine torque can then be solved using equation (2).

$$T = \sigma_{\mathrm{Ftan}} 2\pi r^2 l = \sigma_{\mathrm{Ftan}} 2V, \tag{2}$$

where r is outer radius of rotor surface, l is length of the rotor, and V is the rotor volume. (Pyrhonen, Jokinen & Hrabovcová 2014). This simplification gives easy way of quickly solving rotor volume needed to generate necessary torque in a certain application. Even though available torque is proportional to twice the rotor volume, airgap radius affects more than length. If radius is doubled, active length to produce same amount of torque with same

tangential stress is only one quarter of the original. Larger airgap radius machine is more optimal in reaching higher efficiency and uses less material.

Stator for this type of machines from electromagnetic perspective is same as smaller, higher rotational speed machines. Difference in stator structure comes from assembly, serviceability, and mechanical rigidity. Limiting factor for how thin stator yoke can be is flux density value. With large diameter and high mechanical forces acting on the winding and core, excess core material might be necessary to ensure mechanical rigidity.

Large number of poles is advantageous in large diameter direct driven high torque low speed machines. Increasing pole number increases electrical frequency, decreases stator copper losses, and required stator yoke thickness. Electrical machine synchronous speed n can be determined form equation ((3).

$$n = \frac{60f}{2p}, \tag{3}$$

where f is electrical frequency and p is the number of pole pairs in machine. As equation (*3*) states, electrical frequency increases when pole number increases, when the rotational speed is kept constant. When electrical frequency increases, less winding turns are needed to induce the same value of back-emf E. High pole number also increases the stator slot number which leads to ability to use high number of parallel branches leading to lower stator resistance and copper losses. When stator slot number increases and airgap diameter is kept constant, stator slot pitch becomes narrower. This means that narrower flux path is required to keep the same flux density in the stator yoke. Electrical frequency with variable frequency drives should be kept above 10 Hz in continuous operation to avoid excess IGBT heat cycling stress. Limiting factor for number of poles on the aspect of the stator is that slots need to be wide enough to fit copper bars and to not increase the stator slot leakage flux unnecessarily. (Ruuskanen 2011)

Rotor structure used in high torque low rotating electrical machines must fulfil several demands. Because torque created by the electrical machine comes directly from the magnetic coupling force between stator and rotor, rotor structure must be able to transmit torque created by the force from rotor surface to the shaft. If rotor diameter is large enough,

circumferential velocity becomes high, and structure will experience high mechanical stresses even when rotational speed is low. Bolted and other types of mountings or connections must be able to withstand these forces. Depending on machine use case and topology, high mechanical vibrations might be excited either by some harmonics from stator side, large cogging torque, or load. Mechanical integrity should be ensured by Finite Element Analysis (FEA) before building a prototype to avoid excess costs.

2.2 Permanent Magnet Excited Versus Electrically Excited Synchronous Machines

Synchronous machine rotor poles are either salient or non-salient. Pole is defined as salient pole if there is inductance difference between direct (d)- and quadrature (q)-axis. Rotor d- and q-axes of electrically excited and surface mounted permanent magnet (SPM) synchronous machines are illustrated in Figure 1 below.

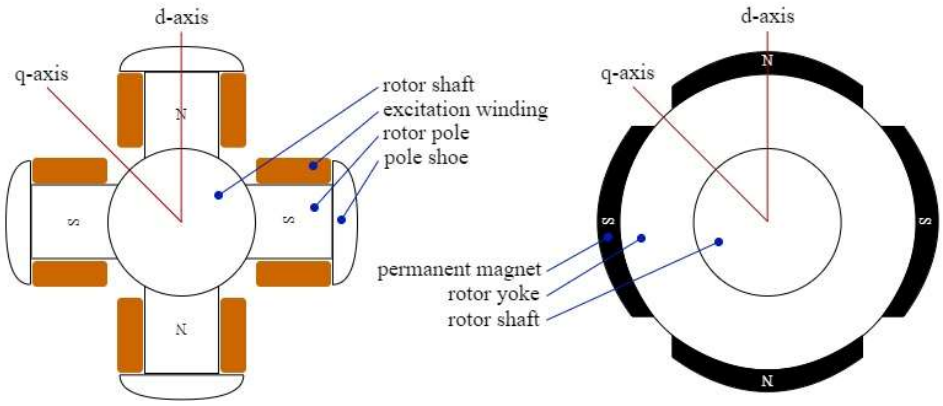

Figure 1. Example 4-pole rotor structures of electrically excited and surface mounted permanent magnet synchronous machines, illustrating d- and q-axes.

As permanent magnet materials have permeability close to permeability of air, with surface mounted permanent magnets, inductances on d- and q-axes are close to identical, and machine can be identified as non-salient pole machine. Electrically excited and interior permanent magnet (IPM) rotors have difference in permeability between d- and q-axes because rotor pole material, for example electrical steel, has different permeability than air. This creates inductance difference between d- and q-axes. Figure 2 presents examples of

interior permanent magnet rotor structures where magnets are mounted tangentially and radially.

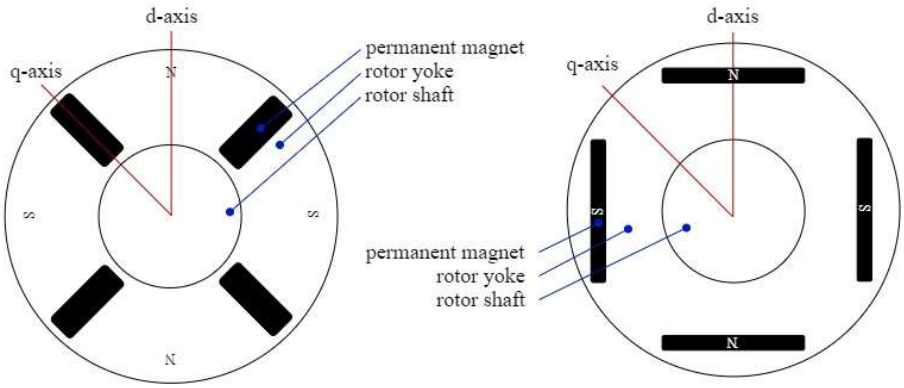

Figure 2. Example 4-pole rotor structures with radially and tangentially mounted permanent magnets with their respective d- and q-axes shown.

From figures 1 and 2 can be seen that electrically excited rotor structure tends to be complicated and has limit on how small it can be designed. To avoid leakage flux between rotor poles, airgap between the rotor poles must be sufficient. Flux route from pole to pole tends to be long which leads to increase in excitation needed to create same amount of rotor flux. Surface permanent magnet mounting on high circumferential speed rotors tends to be tricky. On small diameter rotors, magnets can be glued on rotor surface and retention band is wrapped around the magnets. This is only applicable to small diameters because this creates another issue with different thermal expansion coefficients of materials used and objects expand directly proportionally to the size of the object. The material of the retention band should also be electrically nonconducting or have as high resistivity as possible to avoid eddy current losses on the band and excess heating of rotor. Retention bands are typically made of glass or carbon fibre or stainless steel. Problem with glass or carbon fibre is that they act as thermal insulators and do not expand when heated, this causes excess heating in rotor components and high stress in the band when materials under the band expand. Carbon fibre also suffers from eddy current losses, though resistivity is highly dependent of fibre alignment and the ratio of epoxy resin and fibres. Stainless steel band expand more like different metals used in the rotor but has lower resistivity than fibre options and therefore experiences eddy current losses to some extent.

Machine with permanent magnet rotor has several disadvantages when compared to electrically excited synchronous machine. As rotor flux production is only result of permanent magnets remanence flux, it is not adjustable. This means that machine operates ideally only at the nominal operation point or area where it is optimized. On the other hand, advantage of using permanent magnets as the rotor excitation source means that rotor does not need an external source via slip rings or inductive coupling to be excited. Rotor copper losses are also diminished since there are no windings needed in the rotor, which means increase in efficiency. With removal of the need for slip rings or inductive coupling, results in less need of maintenance.

3 Fractional Slot Concentrated Winding Versus Integer Slot Distributed Winding

In this chapter fractional slot concentrated windings (FSCW) and integer slot windings (ISW) are compared. Comparison parameters includes electromagnetic and mechanical properties and material costs. This gives brief background on differences and technical properties for choosing winding topology. Of course, before final decision of the winding type for a specific machine, electromagnetic simulation must be conducted to ensure electrical and electromagnetic performance. Number of slots per pole and phase q, is a parameter defining winding topology. Parameter q can be solved from equation (4)

$$q = \frac{\frac{Q_s}{2p}}{m}, \tag{4}$$

where Q_s is number of stator slots and m is number of phases. If q is an integer (1, 2…), winding is an integer slot distributed winding. This means that one winding loop spans over 2 or more stator teeth. On the other hand, for example in 10 pole, 12 slot machine, q is a fractional number $\frac{2}{5}$ and one winding loop is concentrated around one stator teeth.

3.1 Electromagnetic Comparison

In this chapter, properties of different winding types are briefly explained. Their main pros and cons are defined, which include winding factor, slot and airgap harmonics, torque ripple and loss distribution.

3.1.1 Winding factor

Winding factor is one of the important parameters to be solved when considering specific winding type. Winding factor is a number between 1 and 0, that describes the voltage inducing capability from the air gap flux density. The higher the winding factor the higher is the induced back electromotive force for a certain amplitude of airgap flux density and number of winding turns. Winding factor ξ_v for symmetrical integer slot winding can be calculated from the equation (*5*)

$$\xi_v = \frac{\sin\left(\frac{v}{p}\,\frac{\pi}{2m}\right)}{q\sin\left(\frac{v}{p}\,\frac{\pi}{2qm}\right)}\sin\left(\frac{v}{p}\,\frac{y}{qm}\,\frac{\pi}{2}\right), \tag{5}$$

where v is harmonic number and y is the coil pitch.

Fractional slot two-layer windings can be divided into 1st- and 2nd-grade windings. 1st- grade fractional slot concentrated two-layer winding has equal number of positive and negative coils in one layer. For example, in 10 pole 12 slot topology, first layer has 2 positive and 2 negative coils. On the other hand, 2nd-grade fractional slot concentrated two-layer winding has unequal number of positive and negative coils in one layer, though it must be noted that second layer must have opposite numbers of positive and negative coils. For example, in 22 pole 21 slot topology, first layer could have 3 positive and 4 negative coils, and second layer then must have 4 positive and 3 negative coils. For 1st-grade concentrated fractional slot winding, winding factor can be solved from equation (*6*)

$$\xi_v = \frac{\sin\left(\frac{v}{p}\,\frac{\pi}{2m}\right)}{nq\sin\left(\frac{v}{p}\,\frac{\pi}{2nqm}\right)}\sin\left(\frac{v}{p}\,\frac{y}{qm}\,\frac{\pi}{2}\right), \tag{6}$$

where n is the denominator of q. For 2nd-grade concentrated fractional slot winding, winding factor can be solved from equation (7)

$$\xi_v = \sin\left(\frac{v}{p}\,\frac{\pi}{2}\right)\frac{\sin\left(\frac{v}{p}\,\frac{\pi}{2m}\right)}{nq\sin\left(\frac{v}{p}\,\frac{\pi}{2nqm}\right)}\cos\left(\frac{v}{p}\,\frac{\eta_v}{2}\right), \tag{7}$$

where η_v is the angle from voltage vector graph. (Salminen 2004).

3.1.2 Loss Distribution

Loss distribution between these two types of permanent magnet machine topologies differ somewhat. Due to the long end windings and less harmonic content in the airgap, losses of integer slot wound machine are mainly copper losses in the stator windings. Copper losses are resistivity losses due to the resistance of the conductor in the winding. Conductor resistance *R* is written as

$$R = \rho_{\mathrm{cu}}\frac{l}{A}, \tag{8}$$

where ρ_{cu} is resistivity of copper, *l* is length of the conductor and *A* is cross-sectional area of the conductor. Equation (*8*) shows that copper losses in the winding are directly proportional to winding loop length. Copper losses for 3-phase machine can be solved using

$$P_{\mathrm{cu}} = 3I^2R_{\mathrm{ph}}, \tag{9}$$

where P_{cu} is copper loss, *I* is the current through winding and R_{ph} is the phase resistance of the winding. For fractional slot concentrated windings, copper losses in stator windings are lower due to shorter end windings. However, rotor losses due to eddy currents in permanent magnets and rotor core are significantly higher than in integer slot winding machine. This difference in loss distribution might help with cooling of the stator, of course keeping in mind also that rotor temperature is kept within the temperature limits set by the magnet

material to avoid demagnetization resulted from excess temperature rise. Therefore, special emphasis must be paid to the rotor cooling. Use of laminated rotor core and axially or radially segmented permanent magnets might be necessary to reduce rotor losses to acceptable level.

In ideal situation synchronous machine would be driven with sinusoidal voltage and has as sinusoidal flux density distribution only with fundamental harmonic in the airgap. This way flux seen by the rotor would be truly sinusoidal and in steady state moving with the stator field and rotor and no eddy current losses are generated due pulsating field. In real life, this situation is not reached and there are always some pulsations in the airgap flux due to supply and slotting harmonics. The generated eddy current losses P_{PM} can be roughly estimated with equation (10).

$$P_{\mathrm{PM}} = \frac{V_{\mathrm{PM}} w_{\mathrm{PM}}{}^2 \hat{B}_{\mathrm{ag}}{}^2 \omega^2}{12 \rho_{\mathrm{PM}}}, \tag{10}$$

where V_{PM} is total volume of magnets, w_{PM} is width of magnet, ω is angular frequency and ρ_{PM} is resistivity of the magnets. (Deeb 2011). Losses due to eddy currents can be reduced by segmentation of the permanent magnets. This makes eddy current paths shorter thus decreasing resistive loss. With Segmentation Reduction Factor (SRF), decrease of eddy currents solved from equation (11).

$$SRF = \frac{l_{\mathrm{seg}}}{l_{\mathrm{seg}} + \tau_{\mathrm{s}}}, \tag{11}$$

where l_{seg} is the length of the permanent magnet segment and τ_{s} is the stator slot pitch. (Suuronen 2019). Effect of segmentation on eddy current path in permanent magnets is illustrated in Figure 3.

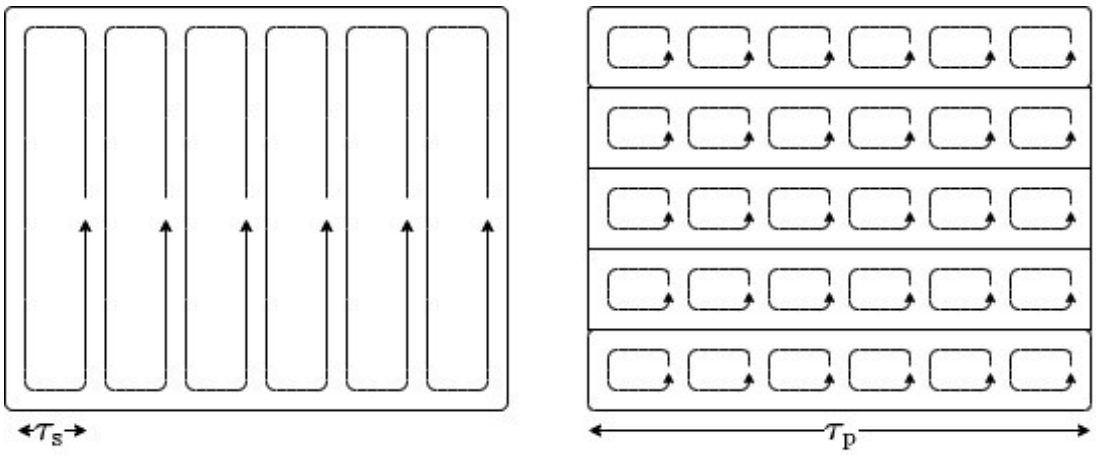

Figure 3. Permanent magnet segmentation effect on eddy current path.

3.2 Mechanical Comparison

Integer slot and fractional slot concentrated windings have several mechanical key differences. First and the most noticeable is the end windings. In ISW $q = 1$, phase U winding loop spans over three stator teeth, needing to dodge V- and W-phases end windings. This winding is illustrated in Figure 4 and end winding is projected isometrically and radially in Figure 5.

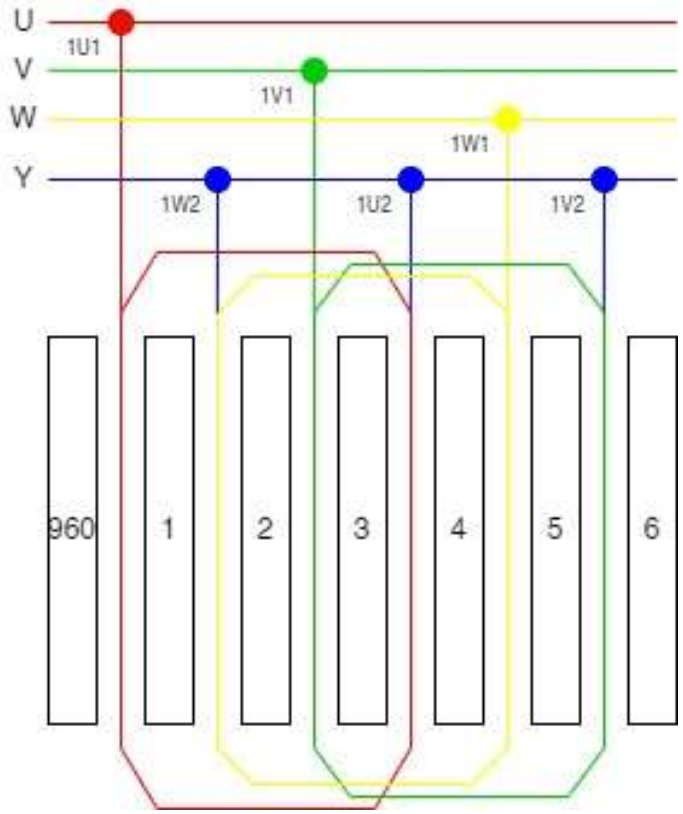

Figure 4. Integer slot winding for machine with q = 1.

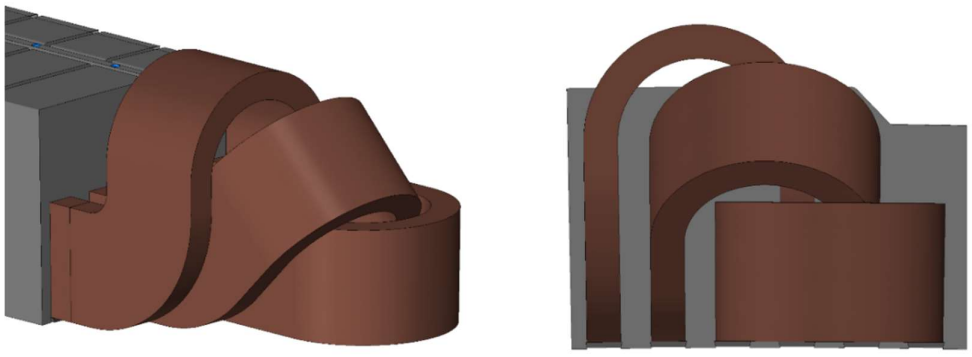

Figure 5. 3D-model illustrating ISW q = 1 end winding, isometric and radial projection (The Switch Engineering Oy, 2023).

As stated earlier fractional slot concentrated winding has significantly shorter end winding than integer slot windings. This is because one winding loop must circle only around one

stator tooth. Fractional slot concentrated winding is illustrated in Figure 6. This winding has two teeth in series and 64 parallel branches. Series connection of the end windings can be done by soldering and insulating after teeth are assembled to frame. End winding is projected isometrically and radially in Figure 7

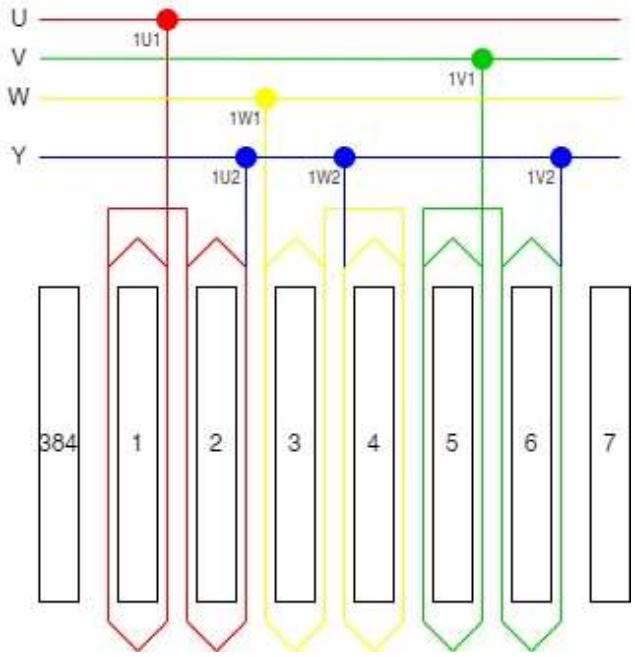

Figure 6. Fractional slot concentrated winding for machine with q = 0.4 and number of parallel branches a = 64.

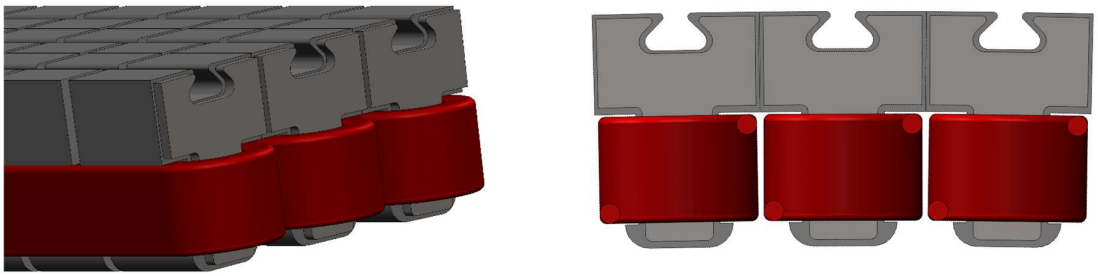

Figure 7. 3D-model illustrating FSCW q = 0.4 end winding, isometric and radial projection (The Switch Engineering Oy, 2023).

Large diameter machine creates several problems which must be considered during machine design process. These problems include mass, flexing of structures during lifting, assembly, and serviceability. Mass creates problem that even if machine could be manufactured in one piece, not all end users have the lifting capacity of hundreds of tons. If mass can be handled as single unit from lifting point of view, structures mechanical rigidity might be a problem as weight spans over a large circular object as the stator, structure might flex over limits or even brake into half. From assembly side, smaller and lighter pieces are typically easier to assemble and handle, this also stands for serviceability. If stator and rotor can be made from smaller pieces, segments, replacement of a single smaller part takes less resources, leads to decreased down-time and production losses. Too small segments mean more joints to make and to align. This can easily make structure too complicated and time consuming to assemble.

4 Design and Calculation Results Comparison

Designing and simulation started by analytical design of the machine. Analytical models give fast, yet reasonably accurate design that can be used for starting of finite element analysis. Parameters for dimensioning are shown in Table 1 below. Additionally, overload point at 10 % of nominal speed with 150 % of nominal torque was set. Analytical model used in preliminary design is made by D.Sc. Jussi Puranen from The Switch Engineering Oy (TSW).

Table 1. Machine design parameters.

Parameter	Value	Unit
Power, P	28	MW
Speed, n	9.61	rpm
Airgap diameter, D_δ	15	m

Tangential stress value in preliminary design was chosen σ_{Ftan} = 56 000 N/m^2 which is based on normal tangential stress values reached with low rotating speed, high torque permanent magnet machines at The Switch (The Switch Engineering Oy, 2023a). Higher values can be reached but relatively loose electromagnetic design gives the ability to reach needed starting torque and better efficiency. This led to rotor volume of 248.4 m^3 which gives axial length of 1.4 m with 15 m airgap diameter.

4.1 Preliminary Simulations and Comparison

Preliminary geometries utilizing both winding concepts were build in FEA. Both concepts had rotor drum made from S355J0- structural steel and permanent magnets with the approximate shape of magnets used in The Switch's magnet modules. N45UH from Yantai Dongxing Magnetic Materials Inc. (YSM) was chosen to be used as permanent magnet material and FLU M400-50A from Altair Flux2D material library as a stator core lamination.

These materials could be changed later during the design process to achieve desired performance and efficiency. Key material properties of N45UH are provided in Table 2.

Table 2. YSM N45UH permanent magnet properties in ambient temperature and adjusted to 75 °C operating temperature.

Parameter	Value	Unit
Average remanence flux, $B_{r,avg}$ [20°C]	1.33	T
Minimum coercive force, H_cJ [20°C]	1989	kA/m
Average remanence flux, $B_{r,avg}$ [75°C]	1.25	T
Minimum coercive force, H_cJ [75°C]	1442	kA/m

Pole pair number p = 160 was chosen as it led to approximate pole pitch τ_p of 146 mm. This also increases electrical frequency from under 10 Hz typically used in electrically excited machines of the same size to 25.63 Hz, which is much more feasible for normal IGBT converter. Nominal voltage U_n was chosen to be 690 V as then normal low voltage converters can be used instead of medium voltage converters. The integer slot design will later be referred as ISW and surface mounted permanent magnet fractional slot concentrated wound design as SPM FSCW. With q = 1 integer slot machine, this pole number resulted in $Q_{s,isw}$ = 960 stator slots and with q = 0.4 fractional slot concentrated machine $Q_{s,fscw}$ = 384 stator slots. Stator slot numbers $Q_{s,isw}$ = 960 and $Q_{s,fscw}$ = 384 results in stator slot pitches of $\tau_{s,isw}$ = 49.11 mm and $\tau_{s,fscw}$ = 122.78 mm, respectively. These are in line with the recommended stator slot pitches 14 to 75 mm for synchronous machines and large PMSMs. (Pyrhonen et al. 2014). It must be noticed that the recommended stator slot pitches for synchronous machines are not directly applicable to fractional slot concentrated windings. Winding turns were adjusted in analytical models in a way that back electromotive forces E_{PM} of both integer slot and fractional slot wound machines would be equal with same permanent magnet material volume, approximately 0.95 x U_n. In permanent magnet synchronous machines, E_{PM} is typically between 0.9 - 1.1 x U_n. Relatively high values of E_{PM} saturates stator teeth heavily, creating excess losses and heat, though relatively low values of E_{PM} will also saturate teeth and all of the supply voltage cannot be used to increase flux (Pyrhonen et. al. 2014).

4.1.1 No-load Simulations and Losses

Geometry was built in Altair Flux2D- FE software package for further analysis. Simulations in preliminary stage of design for both machines included no-load and nominal point operation. In no-load simulation, machines were rotated with nominal speed with high resistance to prevent current flowing in stator windings. This simulates open circuit condition. Parameters used in the simulations are given in Table 3 and simulation results in Table 4. In calculations of copper losses, copper resistivity was adjusted to match 110 °C to consider temperature rise of 70 °C with ambient temperature of 40 °C.

Table 3. No-load simulation parameters for integer slot and fractional slot concentrated winding machines.

Parameter	ISW	SPM FSCW	Unit
Speed, n	9.61	9.61	rpm
Frequency, f	25.63	25.63	Hz
Winding turns, N_s	26.00	30.00	
Parallel braches, a	160.00	64.00	
Magnet relative width, α_{PM}	0.80	0.80	

Table 4. No-load simulation results for integer slot and fractional slot concentrated winding machines.

Parameter	ISW	SPM FSCW	Unit
Cogging torque, T_{cog}	2153.94	105.83	kNm
Back-emf, E_{PM}	654.60	657.78	V
Airgap flux density, B_{ag}	0.989	0.913	T
Stator core loss, P_{st}	66.38	44.31	kW
Additional loss, P_{add}	0.55	1.64	kW
Friction loss, P_{fr}	7.50	7.50	kW
Magnet loss, P_{PM}	33.68	48.02	kW
Rotor yoke loss, P_{rt}	2.22	226.75	kW
Total loss, P_{nl}	110.33	328.22	kW

SPM FSCW machine was shown to have higher permanent magnet losses and unacceptable level of losses in the rotor yoke which is solid structural steel. Eddy current losses could be decreased by slitting surface of the rotor yoke though this leads to increased complexity of the machining and mounting issues for the magnet modules. Average airgap flux density is also lower with the same amount of PM material compared to ISW machine due to higher leakage fluxes. This is also seen as higher number of winding turns to achieve the same level of back electromotive force E_{PM}. Geometries and flux paths in no-load for ISW and FSCW are shown in Figure 8 and Figure 9 respectively. With q = 1 ISW only 1 pole and 3 slots would be enough to meet odd periodicity condition but for illustrative purposes 2 poles are shown in Figure 8. Figure 9 includes 5 poles and 6 slots to show FSCW q = 0.4 odd periodicity completely. FSCW was originally simulated with modelling of all 10 poles and 12 slots. After noticing repeatable pattern on permanent magnet losses, odd symmetry condition with 5 poles and 6 slots was found. Stator geometry must be cut in the middle of the slot to achieve symmetrical model with fractional concentrated winding, as 1 winding loop wraps around one tooth.

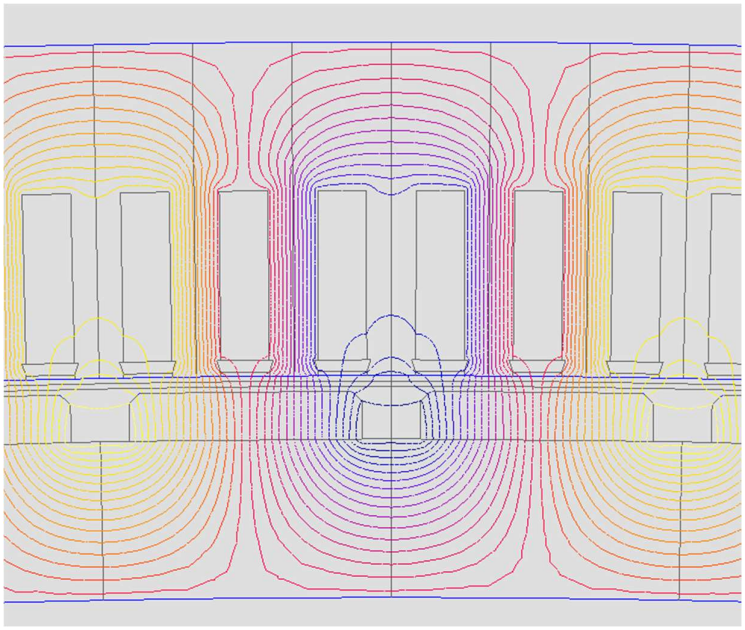

Figure 8. ISW SPM flux paths in no-load operation.

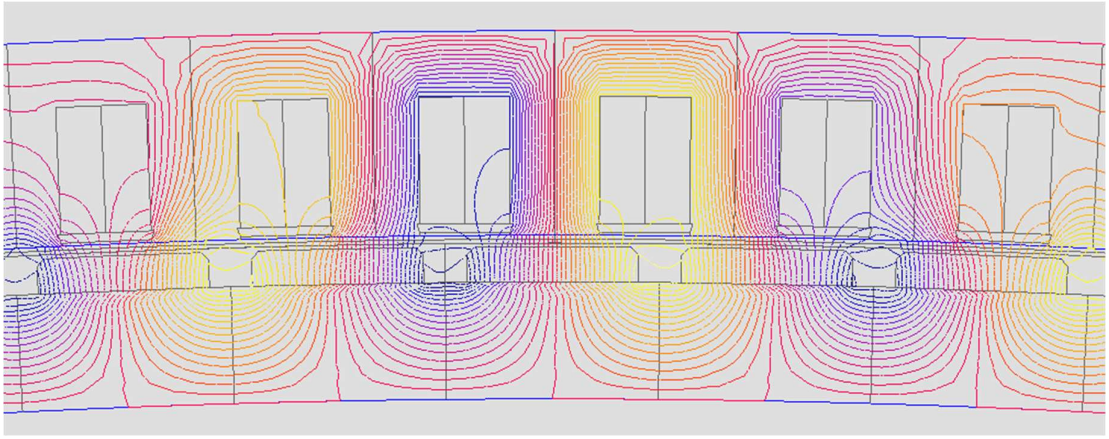

Figure 9. FSCW SPM flux paths in no-load operation.

IPM rotor model is created to reduce rotor losses in the FSCW design, later referred as IPM FSCW. Rotor lamination decreases eddy current losses in same way as permanent magnet segmentation by shortening the eddy current path. The thinner the lamination thickness chosen, the lower the eddy current losses, though thinner lamination costs more than thicker ones. Rotor lamination is chosen to be modelled from the same M400-50A as stator lamination. In later stages if design is seen to be favourable, material choice can be optimized to decrease cost. Interior permanent magnet rotor design can decrease average airgap flux density by even 10 %. This is due to increase in rotor leakage fluxes and increased length of main flux path. Flux barriers consisting of air at the end of the magnets are designed to minimize short circuit effect of permanent magnet flux and thus increases the amount of useful volume of permanent magnet.

Mechanical stresses that effect the rotor lamination and permanent magnets always creates some deformation to the lamination sheets. This is why permanent magnets in IPM rotors should be fixed inside the slot with flexible glue. Gluing also protects magnets from braking due to vibrations and possible hits during installation. Permanent magnet can also be divided along the tangential direction and bridges can be designed between permanent magnet segments to add strength to cope with shear stresses affecting on lamination on top of permanent magnets. Axial length of the permanent magnets should also be considered as longer magnets increase stresses affecting on lamination. IPM pole design and flux paths are illustrated in Figure 10.

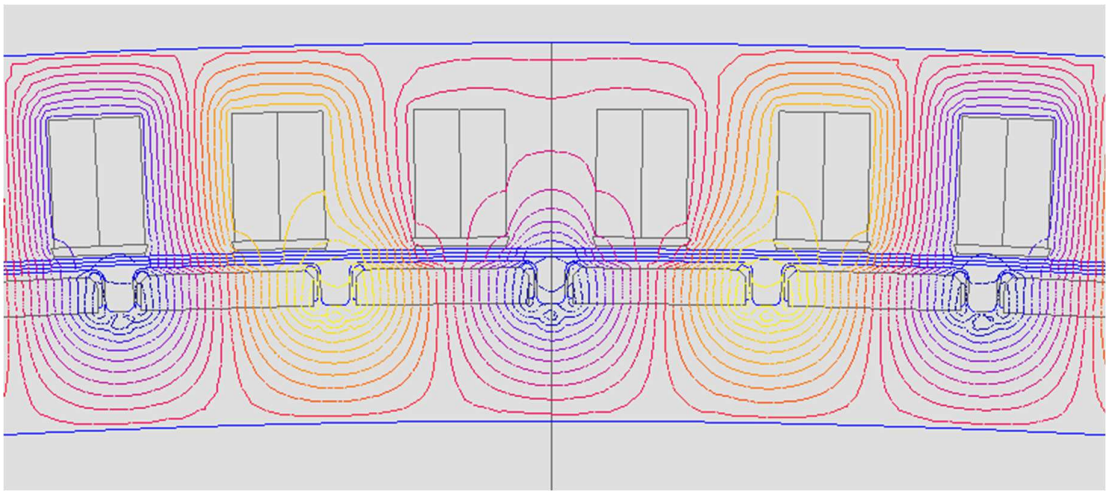

Figure 10. FSCW IPM geometry and flux paths in no-load operation.

IPM design reduced rotor no-load losses dramatically, permanent magnet losses P_{PM} reduced by 82 % and rotor losses in rotor drum P_{dr} by 100 %. Additional rotor losses P_{rt} = 9.83 kW from laminations were added. Machine back electromotive force E_{PM} reduced as airgap flux density decreased. This is due to increased leakage flux between poles via stator teeth and flux short circuit at the end of permanent magnets. Results of IPM FSCW design at no-load are shown in Table 5. Results show significant improvement and no-load losses are just over half of the no-load losses of SPM ISW machine.

Table 5. No-load simulation results for IPM FSCW.

Parameter	IPM FSCW	Unit
Cogging torque, T_{cog}	105.83	kNm
Back-emf, E_{PM}	657.78	V
Airgap flux density, B_{ag}	0.838	T
Stator core loss, P_{st}	39.27	kW
Additional loss, P_{add}	0.31	kW
Friction loss, P_{fr}	7.50	kW
Magnet loss, P_{PM}	5.60	kW
Rotor loss, P_{rt}	9.83	kW
Total loss, P_{nl}	62.52	kW

Airgap flux distribution between ISW and FSCW differs a lot. Airgap flux distribution and their harmonic contents greatly effects on rotor losses and torque quality of the machine. Airgap harmonics of the three different designs are shown in Figure 11.

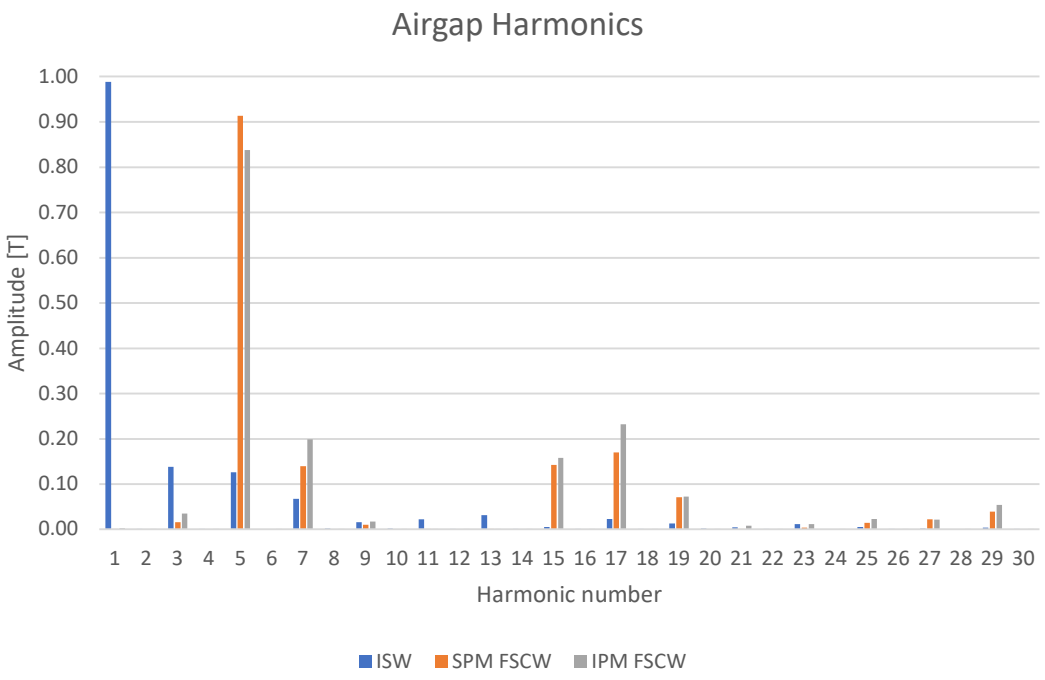

Figure 11. ISW, SPM FSCW and IPM FSCW airgap harmonics.

ISW airgap flux harmonics has fundamental torque producing harmonic number 1 but also includes 3rd, 5th, and 7th with noticeable amplitudes. FSCW designs based on 10-pole 12-slot combination, have fundamental torque producing harmonic number 5. 7th- harmonic is counter rotating and creates losses in the machine. Noticeable amplitudes are seen on 15th-, 17th- and 19th-harmonics. Flux distribution of ISW design is illustrated in Figure 12.

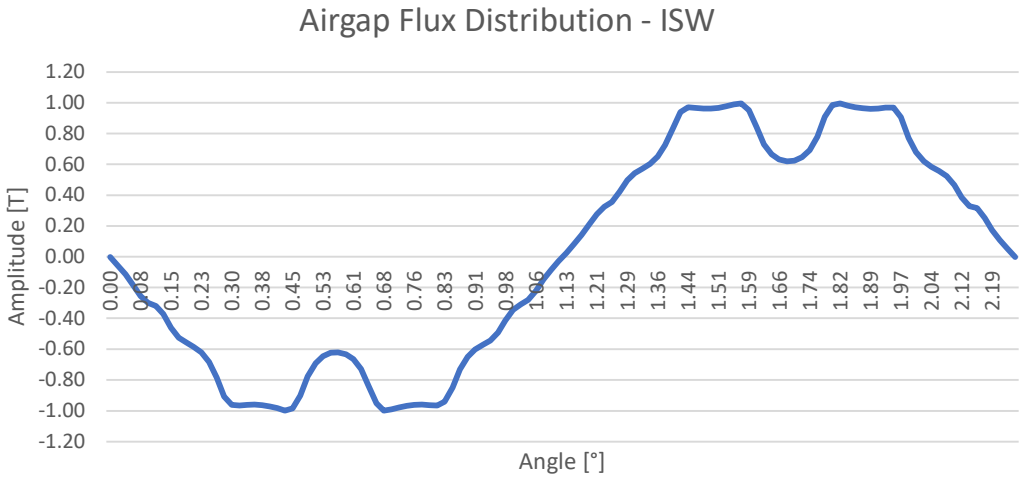

Figure 12. Airgap flux density distribution of ISW design along one pole pair.

Airgap flux distribution of the ISW design shows dramatic slotting effect and differs from ideal sinusoidal airgap flux distribution greatly. Skewing is an effective way of modifying airgap flux distribution form to sinusoidal. It can be done by axially twisting slots by predefined angle or stepping of the row of magnets in the rotor pole. Adverse effect of skewing is that it simultaneously decreases back-emf and peak torque output of the machine. Airgap flux distribution of FSCW designs are illustrated in Figure 13 for SPM and in Figure 14 for IPM.

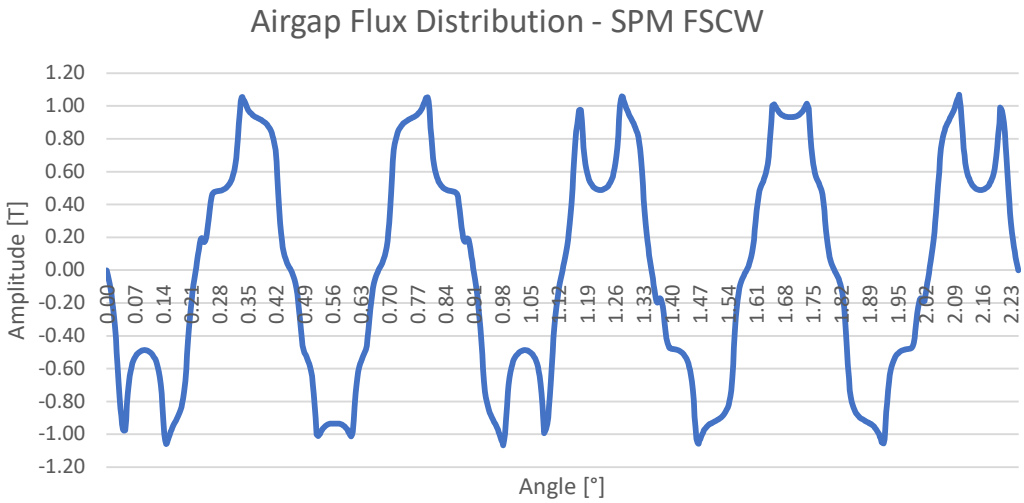

Figure 13. Airgap flux density distribution of SPM FSCW design along one symmetry plane.

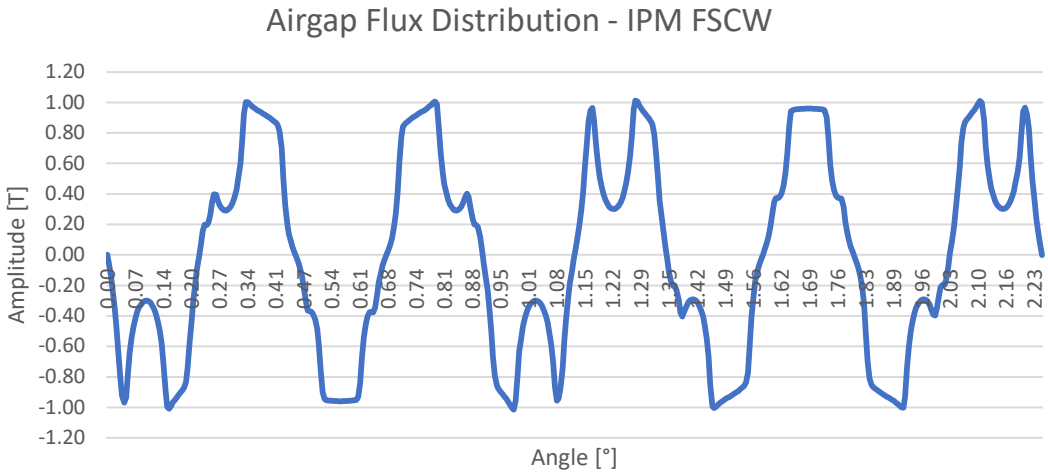

Figure 14. Airgap flux density distribution of IPM FSCW design along one symmetry plane.

Both FSCW designs show similar airgap flux distribution as they are based on the same winding topology, though differences are seen with slightly lower peak amplitudes on IPM design due to leakage fluxes. The odd periodicity condition can be seen if FSCW flux distribution figure is cut in half and end part is turned 180°.

4.1.2 Nominal Point Simulations

All three machine designs were simulated at nominal operation point though SPM FSCW machine is kept only as reference since the rotor losses would require special cooling solutions. These simulations are done to estimate torque characteristics and losses of the machine. Modelled machines are supplied by sinusoidal voltage supply and simulated until steady state has been reached. This simulation yields machine losses, excluding PWM, friction, and mechanical losses. Simulation of PWM losses with voltage supply is complex and highly time consuming. Usually, PWM losses are simulated with current supply as model reaches steady state immediately. PWM can be simulated by adding 3 % of nominal current amplitude with switching frequency on top of the nominal current waveform. (The Switch Engineering Oy, 2023a). Use of voltage supply is more precise but involves transients that take time to become steady before results should be analysed. Simulation results of nominal operation point with sinusoidal voltage supply are shown in Table 6.

Table 6. Results of nominal operation point with sinusoidal voltage supply.

Parameter	ISW	SPM FSCW	IPM FSCW	Unit
Torque ripple, T_{rip}	2090.38	165.89	404.81	kNm
Terminal voltage, U_n	690.00	690.00	690.00	V
Current, I_n	25458.00	26344.00	27830	A
Power factor, $cos\varphi$	0.94	0.93	0.86	
Current density, j	2.89	3.00	3.17	A/mm^2
Stator copper loss, P_{cu}	510.95	487.99	544.60	kW
Stator core loss, P_{st}	72.71	49.36	54.85	kW
Additional loss, P_{add}	84.00	84.00	84.00	kW
Friction loss, P_{fr}	7.50	7.50	7.50	kW
Rotor core loss, P_{rt}	0.00	0.00	11.07	kW
Magnet loss, P_{PM}	38.21	86.08	46.92	kW
Rotor drum loss, P_{dr}	1.64	621.27	0.00	kW
Input power, P_{el}	28715.01	29336.20	28748.95	kW
Total loss, P_h	715.01	1336.20	748.95	kW
Efficiency, η	97.51	95.45	97.39	%

IPM FSCW machine had significant improvement on efficiency compared to the SPM-version. Eddy current losses in rotor drum were totally mitigated by the rotor lamination. Permanent magnet losses were also reduced significantly. With the first iteration of the design, machine efficiency was only slightly lower than in the case of the ISW-design.

4.2 FSCW with Interior Permanent Magnets

Fractional slot concentrated wound machine was seen to have significant improvements in terms of losses with interior permanent magnet rotor. Benefits of simple stator and winding design led to further optimization of the topology in this use case. There are several ways to improve permanent magnet machine efficiency when machine speed, power and pole pair number are set. Increasing airgap flux density by adding more permanent magnet material, reducing magnetic loading, and adding copper in the stator winding. Some improvements

can also be achieved by optimization of rotor pole and stator tooth designs. Rotor pole leakage flux via stator tooth seemed to be major contributor to low air gap flux density. This can be reduced by decreasing relative magnet width α_p or narrowing stator tooth width. Decreasing relative magnet width increases magnetic circuit length from pole to pole, decreasing flux leakage, but it reduces magnet volume which, on the other hand, reduces airgap flux density if not compensated by magnet height. Cogging torque is also affected by α_p (Kurronen 2003), but it is not considered as main optimizable parameter during this thesis. Narrowing stator tooth width also decreases pole to pole leakage flux on the rotor side and decreases slot leakage flux from stator tooth to tooth. Disadvantage is increase in stator tooth flux density which leads to higher tooth core losses. Narrower stator tooth reduces heat transfer from stator winding through the teeth as heat flux path is narrowed simultaneously. (Rilla 2012). Main leakage flux paths are illustrated in Figure 15.

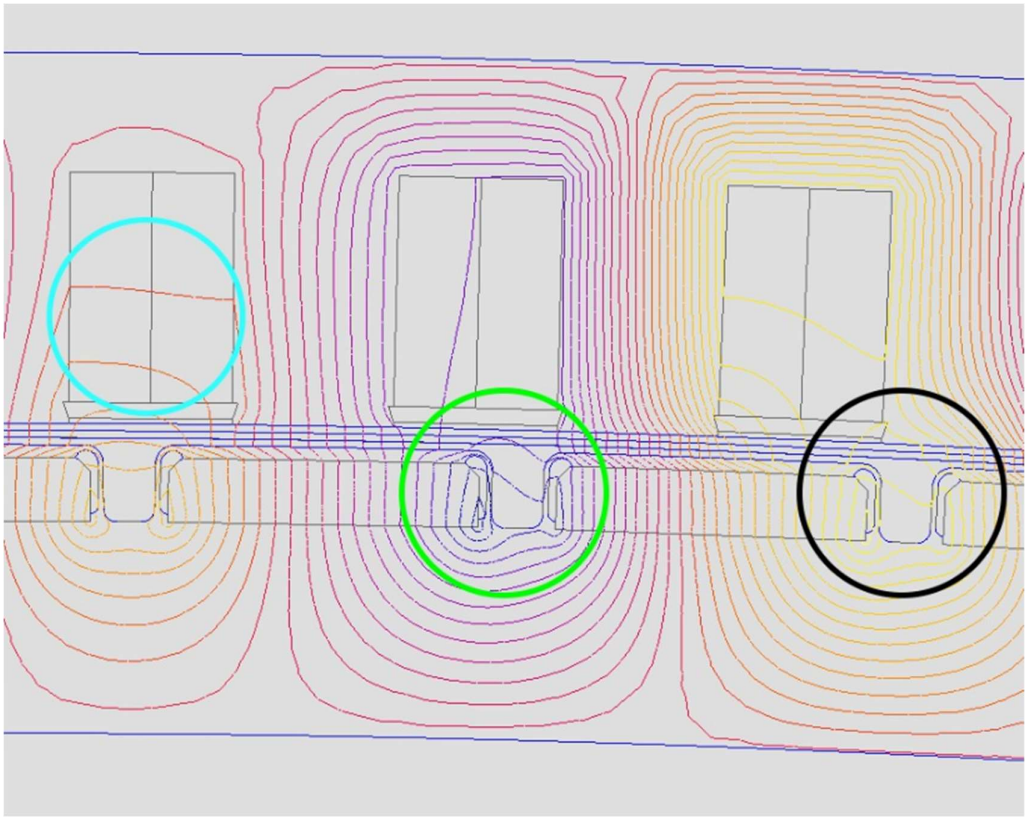

Figure 15. IPM FSCW main leakage flux paths in no-load operation point.

4.2.1 No-load Simulation

Optimization started with creating two different iterations of the IPM FSCW design. First one will have increased amount of permanent magnet material (AddMag) and second where copper mass was increased (AddCu) by means increasing cross-sectional area. Amount of permanent magnet was increased in a way that E_{PM} would match the same level as was in the ISW design, this will decrease the current of the machine at nominal point and decrease copper losses. Possible disadvantage is the addition of eddy current losses in the permanent magnets, but this can be tackled with smaller segmentation. Permanent magnet material was increased by 12 % to reach the same E_{PM}. The second design optimization where copper mass is added, will reduce copper losses as resistance of the winding loop decreases directly proportionally to the phase resistance as described in equation (9). Copper was increased by 2.4 % to reach the same copper loss level as the ISW. After these simulations were done in no-load, third model (Combined) that combines the two previous design optimizations were created. No-load results of the three simulations are shown in Table 7.

Table 7. FSCW no-load results of optimized designs.

Parameter	AddMag	AddCu	Combined	Unit
Cogging torque, T_{cog}	58.78	22.05	24.03	kNm
Back-emf, E_{PM}	654.69	627.26	642.59	V
Stator core loss, P_{st}	45.14	42.70	46.86	kW
Additional loss, P_{add}	0.36	0.34	0.37	kW
Friction loss, P_{fr}	7.50	7.50	7.50	kW
Magnet loss, P_{PM}	9.18	8.78	9.18	kW
Rotor loss, P_{rt}	8.87	8.22	9.25	kW
Total loss, P_{nl}	71.05	67.54	73.16	kW

Addition of permanent magnet material increased flux density in stator and rotor cores, this is shown in increased losses. Addition of copper mass also increased losses through the machine structure because of lengthened flux path, though increase was more marginal. In the model that combined both, increase in no-load losses was the highest as expected.

4.2.2 Nominal Point Simulation

Nominal point simulations for these improved FSCW designs were conducted to evaluate their properties and improvements under load. Simulation results for all three designs are given in Table 8.

Table 8. FSCW nominal operation point simulation results of optimized designs.

Parameter	AddMag	AddCu	Combined	Unit
Torque ripple, T_{rip}	474.66	402.56	342.11	kNm
Terminal voltage, U_n	690.00	690.00	690.00	V
Current, I_n	26527.00	27507.43	26930.00	A
Power factor, $cos\varphi$	0.91	0.87	0.89	
Current density, j	3.03	2.86	2.80	A/mm^2
Stator copper loss, P_{cu}	494.80	485.86	465.69	kW
Stator core loss, P_{st}	56.26	58.54	59.20	kW
Additional loss, P_{add}	84.00	84.00	84.00	kW
Friction loss, P_{fr}	7.50	7.50	7.50	kW
Rotor core loss, P_{rt}	13.23	12.46	12.84	kW
Magnet loss, P_{PM}	46.29	43.65	50.06	kW
Rotor drum loss, P_{dr}	0.03	0.03	0.03	kW
Input power, P_{el}	28702.10	28692.04	28679.31	kW
Total loss, P_h	702.10	692.04	679.31	kW
Efficiency, η	97.55	97.59	97.63	%

Addition of magnet material to achieve the same back-emf E_{PM} as the first ISW design, show decreased stator copper losses P_{cu} due to lower current drawn by the machine. Stator core loss increase is negligible. Rotor core loss P_{rt} and magnet loss P_{PM} stayed in similar levels as the first design. Efficiency level increased to same as with the ISW design. Second improved design with addition of copper material to reduce stator copper losses P_{cu} to same level as ISW design, showed small increase in stator core loss P_{st} due to longer flux path and increased inductance. Rotor core loss P_{rt} and magnet loss P_{PM} decreased when compared to

design with added permanent magnet material. This is due to lower flux density in rotor core and less permanent magnet material. Efficiency is higher than in the AddMag-design. Combined model seemed to have negative effect on stator core loss P_{st} and magnet loss P_{PM}. Though combination of increased winding turn cross-sectional area and airgap flux density decreased stator copper loss significantly from the first design. Permanent magnet loss increased to some degree, but this could be mitigated with smaller segmentation of the permanent magnets. Efficiency improvement was again achieved.

4.3 Comparison of the Machine Designs

When comparing electromagnetic and mechanical aspects of the entire machine, several factors and limitations must be considered. Electromagnetic differences effect on efficiency, losses, torque production capabilities and torque quality and, on the other hand, mechanical aspects effect on manufacturability, serviceability, and transportation of the machine.

Electromagnetically the presented designs differ somewhat and have different advantages compared to each other. In ISW design, end winding losses are almost 28 % of the copper losses, compared to FSCW's 12 %. Large slot openings and FSCW's high winding harmonic amplitudes especially 7^{th}-harmonic leads to the use of laminated rotor structure to mitigate and reduce losses in the magnets and in solid steel rotor drum. Use of laminated rotor structure reduces airgap flux density by c. 10 % and decreased back-emf increases machine current with same amount winding turns.

Mechanically on the stator side, FSCW design has advantage, because it can be assembled in single tooth segments to the subassembly frame. Winding is easier as it can be wound straight around the tooth and all loops are the same. In the ISW design, three different form windings need to be wound on a specific jig and then these pre-wound loops are pressed to stator lamination segment that has slot count divisible by 6 (e.g., 6, 12, 18... slots). On the rotor side, FSCW can be assembled one pole or one pole pair at the time. Lamination can be stacked, and magnets are installed to the slots beforehand and then assembled in smaller segments around the rotor drum. New tooling and instructions need to be done for the manufacturing and assembly. ISW has significant advantage because magnet modules can be used. Magnet module assembly tooling is already made, existing tooling for mounting

can be modified for use on the field and magnet module design has already proven to be robust yet simple.

4.4 Design Optimization and Simulations

Final machine topology was chosen to be ISW $q = 1$ machine with TSW magnet modules. Final design phase includes optimization of machine active length, permanent magnet shape and material, and winding. Geometry is modelled with the magnet module with stainless steel cover. Module consists of 3 permanent magnets each. Machine active axial length was increased by 70 mm to match rotor length using 7 magnet modules. Increase in active axial length decreases machine load angle and current at nominal operation point and increases pull-out torque capacity when airgap diameter was kept constant. Machine total length was increased by 210 mm to consider cooling method of the machine. Permanent magnet material grade could be lowered to N42SH which reduces material costs significantly (The Switch Engineering Oy, 2023b). The new winding was calculated with winding turns increased from 26 to 27 turns. Cross-sectional area of the conductor was increased by 40 % to compensate for increased winding turn length and added winding turn. From Computational Fluid Dynamics (CFD), friction losses in the airgap were calculated to be 0.24 kW instead of analytically estimated 7.50 kW. This is due to slow rotational speed and relatively long airgap.

Optimal relative magnet width was investigated to balance between permanent magnet material effective usage and cogging torque even though cogging torque was not the main optimizable parameter as stated earlier. When permanent magnet volume is kept the same, altering the relative magnet width impacts on airgap flux density, induced back-emf and cogging torque. Decreasing relative magnet width increases magnetic circuit length from pole to pole, decreasing flux leakage, but reduces magnet volume which then again reduces airgap flux density if not compensated by magnet height. Increasing relative magnet width has the opposite effect. Results are given in

Table 9.

Table 9. Results of varying relative magnet width αp

α_p	w_{mag} [mm]	h_{mag} [mm]	B_{ag} [T]	E_{PM} [V]	T_{cog} [kNm]
0.758	111.50	25.83	0.949	625.27	595.30
0.786	115.75	24.88	0.952	629.16	1710.33
0.815	120.00	24.00	0.957	632.29	2615.41
0.844	124.25	23.18	0.958	634.69	3280.78
0.873	128.50	22.41	0.958	636.14	3738.70

Varying relative magnet width α_p had almost linear effect on back-emf and lowest cogging torque value was achieved with lowest relative magnet width. Torque output is considered smooth in traction applications when torque ripple is less than 1-2 % of nominal torque (Rilla 2012). Even though cogging torque does not consider load conditions, it gives some approximation on torque ripple under load and effects starting of the machine. Too high values on the other hand might be troublesome for mechanical rigidity of the machine. With these in mind, desired cogging torque value was set between 5-10 % of nominal.

4.4.1 No-load Simulation

No-load simulation was conducted to the optimized ISW design. In the final simulation results, magnet module losses are included in the rotor losses for simplification. Results are shown in Table 10.

Table 10. ISW with magnet modules. Final simulation results no-load operation point.

Parameter	ISW	Unit
Cogging torque, T_{cog}	1713.50	kNm
Back-emf, E_{PM}	677.15	V
Stator core loss, P_{st}	77.11	kW
Additional loss, P_{add}	0.70	kW
Friction loss, P_{fr}	0.24	kW
Magnet module loss, P_{mm}	22.19	kW
Magnet loss, P_{PM}	30.27	kW
Rotor loss, P_{rt}	2.25	kW
Total loss, P_{nl}	132.76	kW

In the final design, machine back-emf E_{PM} is 0.98 x U_n. Stator core losses increased by 16 % compared to original ISW design due to increased flux path length on stator side. Rotor losses increased by 22.22 kW, because of eddy current losses on the modelled stainless steel magnet module cover.

4.4.1 Nominal Point Simulation

Nominal point simulation was conducted to the optimized ISW design. Machine operation was simulated with sinusoidal voltage (SinU) and current (SinI) supplies. PWM losses were simulated with previously mentioned method by adding 3 % of nominal current amplitude on top of the sinusoidal current waveform with switching frequency of 2.5 kHz. This method is also used later in overload simulations.

Table 11. ISW with magnet modules. Final simulation results at nominal operation point.

Parameter	SinI	PWMI	SinU	Unit
Torque ripple, T_{rip}	2019.70	-	1770.92	kNm
Terminal voltage, U_n	690.50	690.50	690.00	V
Current, I_n	24950	24950	24838	A
Power factor, $cos\varphi$	0.96	0.96	0.97	
Current density, j	2.10	2.10	2.09	A/mm^2
Stator copper loss, P_{cu}	489.40	489.40	484.99	kW
Stator core loss, P_{st}	79.98	93.30	80.63	kW
Additional loss, P_{add}	84.00	84.00	84.00	kW
Friction loss, P_{fr}	0.24	0.24	0.24	kW
Magnet module loss, P_{mm}	22.18	37.44	22.77	kW
Magnet loss, P_{PM}	29.19	60.80	31.32	kW
Rotor drum loss, P_{dr}	1.45	5.17	0.15	kW
Input power, P_{el}	28706.45	28770.34	28704.10	kW
Total loss, P_h	706.45	770.34	704.10	kW
Efficiency, η	97.54	97.32	97.55	%

Machine efficiency with sinusoidal voltage and current supplies corresponded well together with error of 0.3 % between them on the losses. When PWM losses are taken into account, efficiency decreased slightly as expected.

4.4.2 Overload Simulation

Overload capability of the machine needs to be verified to ensure successful starting of the machine. As previously stated, the machine must be capable to produce 150 % of nominal torque at 10 % of the nominal speed. Machine pull out torque with nominal supply voltage at nominal speed is approximately 53100 kNm. This is 1.91 times the nominal torque. At lower speed operation, boosted supply voltage can be used to produce the required starting torque with less current. Results of the overload point simulation are shown in Table 12.

Table 12. ISW with magnet modules. Final simulation results at overload operation point with reduced speed.

Parameter	SinI	PWMI	SinU	Unit
Torque ripple, T_{rip}	2019.70	-	1770.92	kNm
Terminal voltage, U_n	85.47	85.47	85.47	V
Current, I_n	39790.00	39790.00	38954.04	A
Power factor, $cos\varphi$	0.91	0.91	0.92	
Current density, j	3.35	3.35	3.27	A/mm^2
Stator copper loss, P_{cu}	1111.30	1111.30	1065.10	kW
Stator core loss, P_{st}	6.93	33.21	6.93	kW
Additional loss, P_{add}	21.00	21.00	21.00	kW
Friction loss, P_{fr}	0.00	0.00	0.00	kW
Magnet module loss, P_{mm}	0.30	29.20	0.30	kW
Magnet loss, P_{PM}	0.46	56.25	0.44	kW
Rotor drum loss, P_{dr}	0.03	9.91	0.01	kW
Input power, P_{el}	5340.03	5460.87	5293.78	kW
Total loss, P_h	1140.03	1260.87	1093.78	kW
Efficiency, η	78.65	76.91	79.34	%

Machine efficiency suffers greatly at this overload point due to the low power as torque is produced at low speed and relatively high current. Due to the high current, copper losses are clearly dominant. PWM creates most of the losses in the stator core, permanent magnets, magnet module and rotor drum. During PWM simulation, it is important to adjust time stepping interval to compensate for decreased electrical frequency.

4.4.1 Short Circuit Simulation and Demagnetization Evaluation

Short circuit simulations are conducted to determine short circuit current, torque peak and demagnetization risk. In the simulation, machine is rotated at rated speed and switches are closed at certain time to simulate short circuit at machine terminals. Circuit diagram used in short circuit simulations is illustrated in Figure 16.

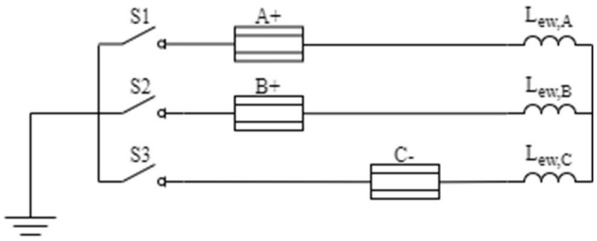

Figure 16. Short circuit simulation circuit diagram.

Coil conductors A+, B+ and C- are corresponding to the modelled three phase windings of the machine. $L_{ew,\,A}$, $L_{ew,\,B}$ and $L_{ew,\,C}$ are corresponding to the end winding inductances of each face. Switches S1, S2 and S3 simulate open circuit and short circuit resistances at machine terminals. In three-phase short circuit simulation switches are closed when one phase back-emf E_{PM} is at zero and in two-phase short circuit simulation two of the three switches are closed when the healthy phase back-emf E_{PM} is at peak value. (Rosu, Saitz & Arkkio 2005). This is the moment in both short circuit conditions when maximum amount of magnetic energy is stored in the circuit leading to highest peak values of current I_{SC}, torque T_{SC} and demagnetization field strengths H_{SC}. Simulations are done with cold (T_{PM} = 20°C) and hot (T_{PM} = 70 °C) machine states. Cold state results in highest current, torque and demagnetization field strength values and hot state results in lowest coercive forces H_cJ in the permanent magnets, lower the coercive force, the higher the risk of permanent demagnetization. Simulation results for two-phase cold short circuit torque, current and demagnetization field strengths are illustrated in Figure 17, Figure 18 and Figure 19 respectively.

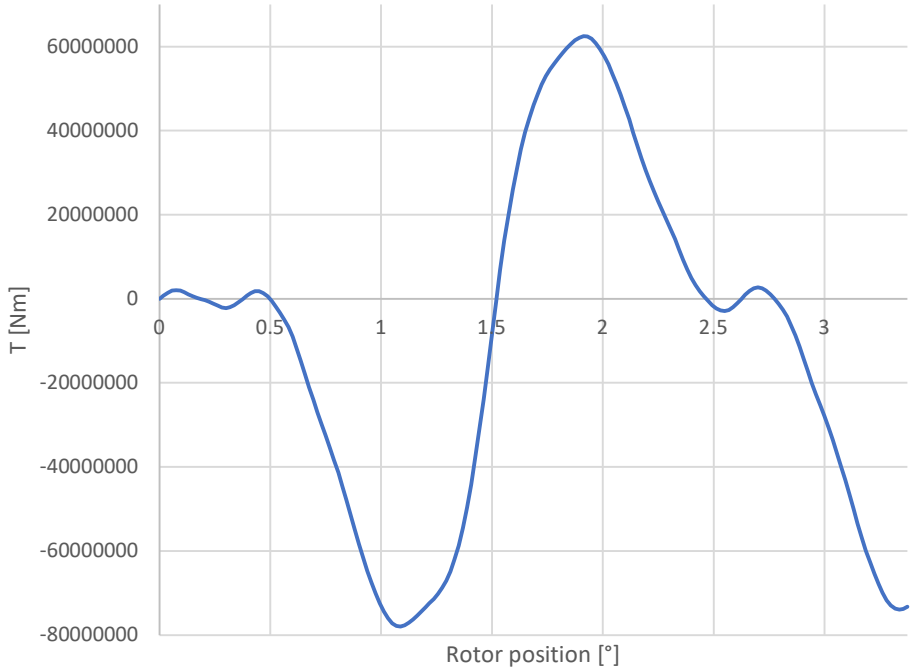

Figure 17. Two-phase short circuit torque $T_{SC,2\text{-}ph}$ for cold machine (T_{PM} = 20°C). Maximum peak value is -77943 kNm

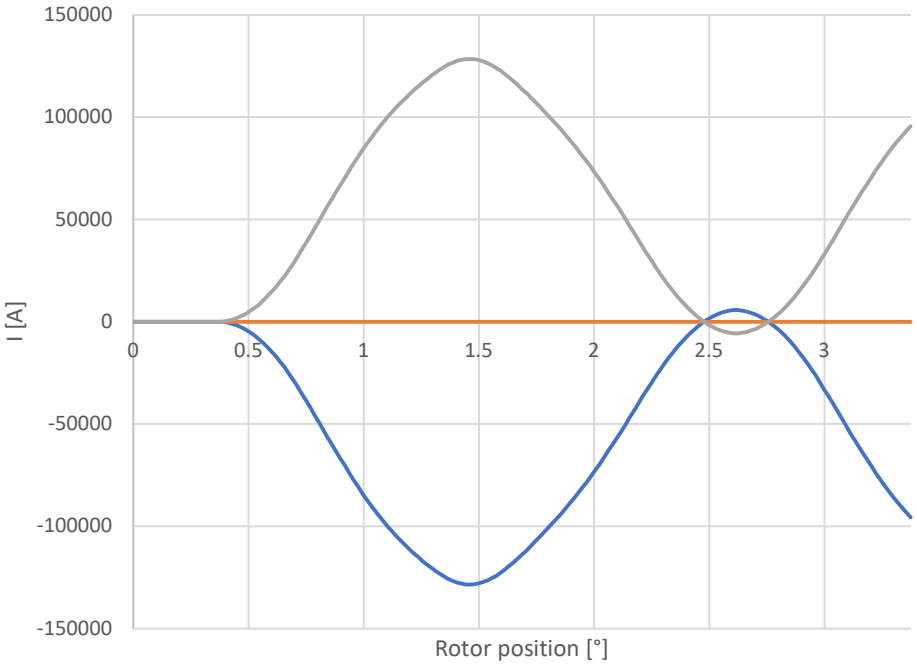

Figure 18. Two-phase short circuit current $I_{SC,2\text{-}ph}$ for cold machine (T_{PM} = 20°C). Maximum peak value is 128.5 kA.

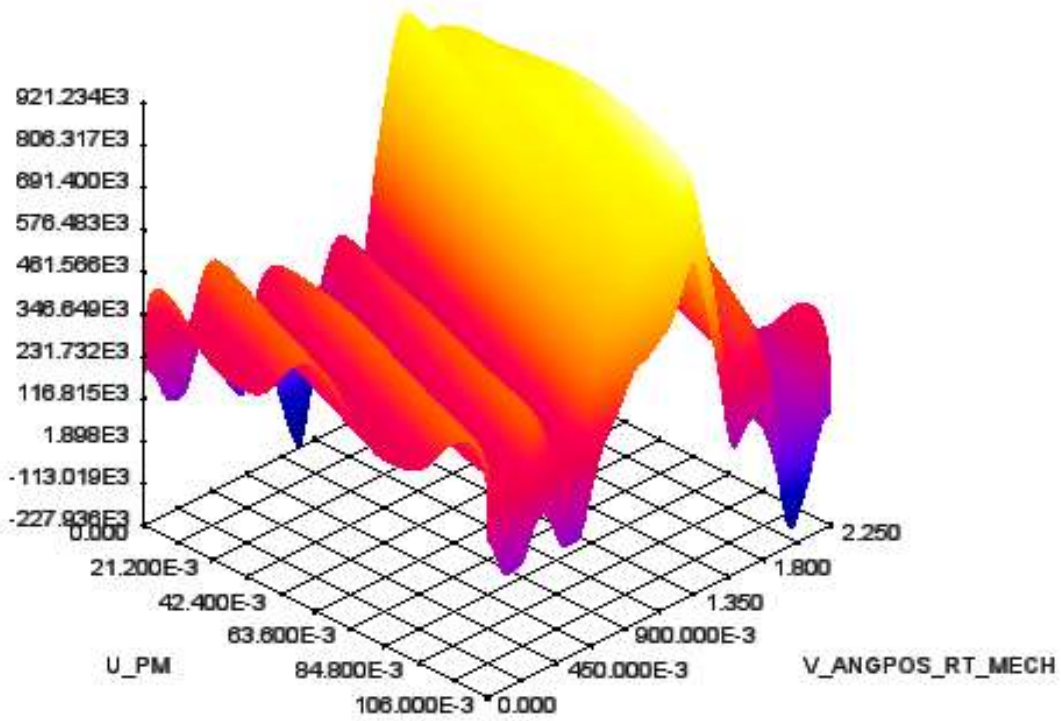

Figure 19. Demagnetizing field strength $H_{SC,2\text{-}ph}$ during two-phase short circuit with cold machine (T_{PM} = 20°C). Worst case field strength is 921 kA/m.

Cold state two-phase short circuit simulations showed that there is no risk of demagnetization in the permanent magnets if machine experiences two-phase short circuit at the worst possible time. Machine will experience high torque and current peaks, and these should be considered during design of electrical protections and mechanical structure of the machine.

Simulation results for three-phase cold short circuit torque, current and demagnetization field strengths are illustrated in Figure 20, Figure 21 and Figure 22 respectively.

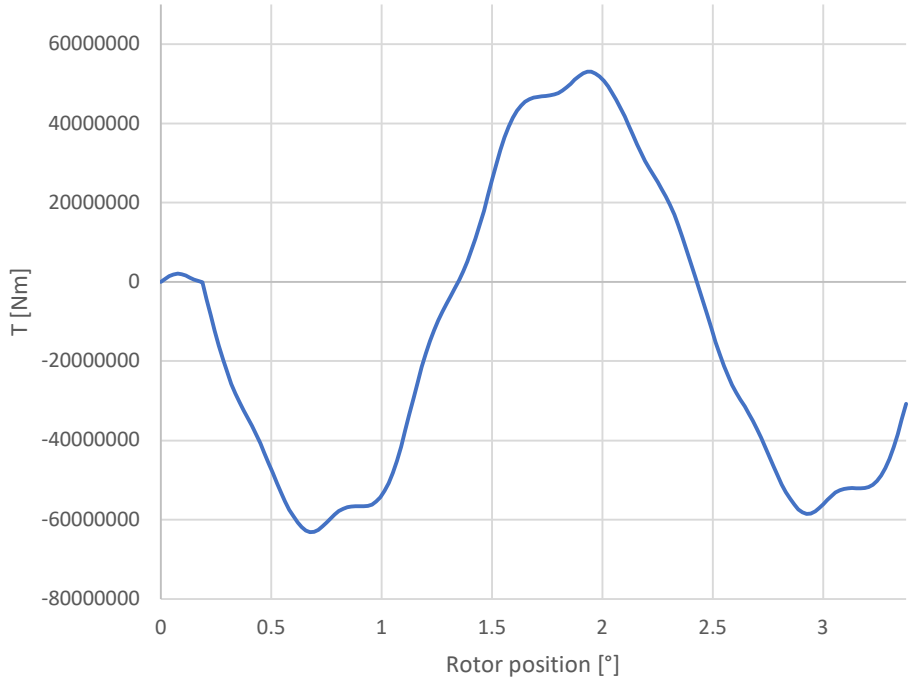

Figure 20. Three-phase short circuit torque for cold machine (T_{PM} = 20°C). Maximum peak value is -63153 kNm.

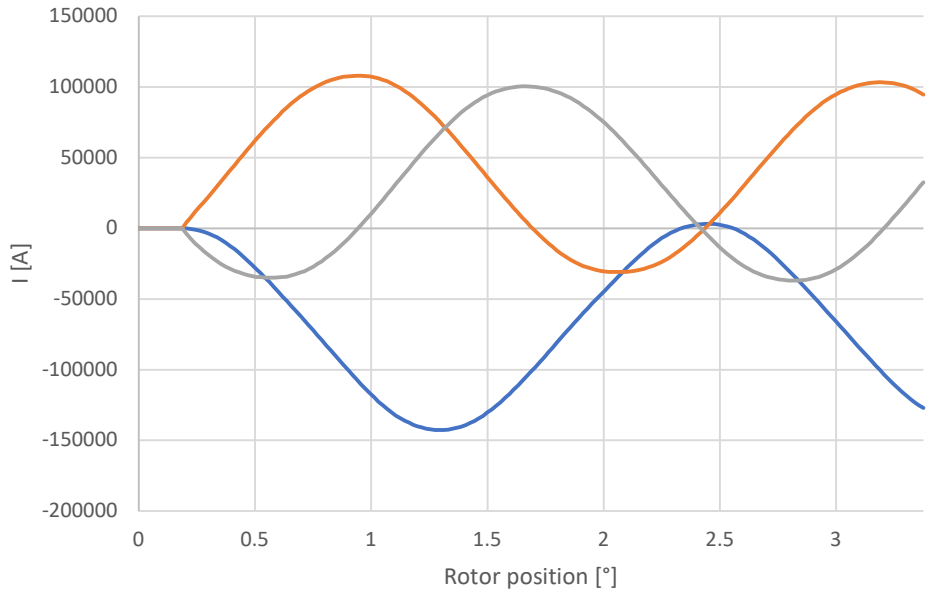

Figure 21. Three-phase short circuit current for cold machine (T_{PM} = 20°C). Maximum peak value is 142.7 kA.

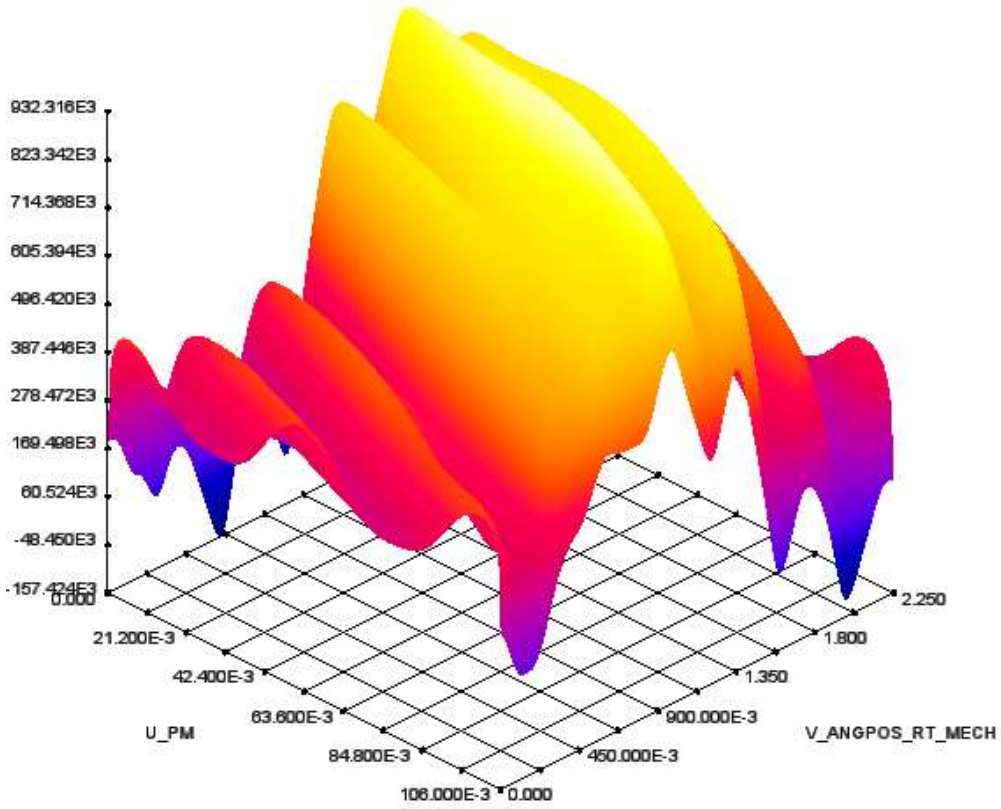

Figure 22. Demagnetizing field strength during three-phase short circuit with cold machine (T_{PM} = 20°C). Worst case field strength is 932 kA/m.

Cold state three-phase short circuit simulations showed that there is no risk of demagnetization in the permanent magnets if machine experiences three-phase short circuit at the worst possible time. Cold three-phase short circuit is even higher than the two-phase short circuit current at $I_{SC,3\text{-}ph}$ = 142.7 kA.

From hot state three-phase short circuit simulation steady state short circuit current RMS-value I_{SC} can be used to calculate d-axis synchronous inductance L_d when angular frequency ω and back-emf E_{PM} are known. The d-axis synchronous inductance L_d can be solved using equation (12).

$$L_d = \frac{E_{PM}}{\omega I_{sc}} = \frac{391.4\ \text{V}}{2 * \pi * 25.63\ \text{Hz} * 45185\ \text{A}} = 53.8\ \mu\text{H} \tag{12}$$

Machine simulated three-phase short circuit current is illustrated in Figure 23. Simulation was run until steady state was reached. Demagnetizing field strengths and minimum coercive force comparison is presented in Table 13 for all 4 short circuit simulations.

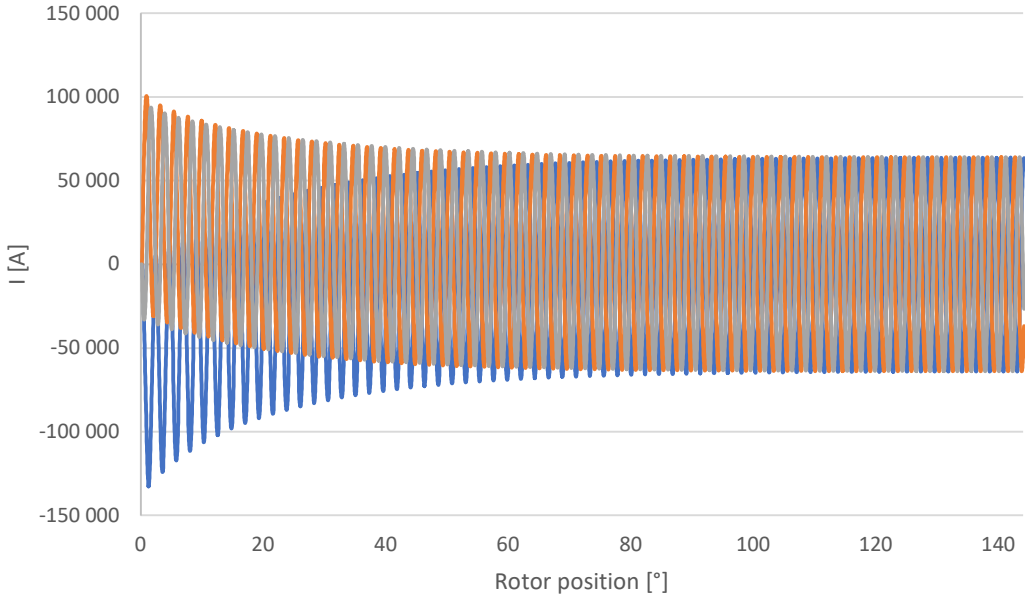

Figure 23. Three phase short circuit currents with hot machine (TPM = 70 °C). Steady state short circuit current value is 45185 ARMS.

Table 13. Two- and three-phase simulated short circuit demagnetizing field strengths and permanent magnet minimum coercive forces at cold and hot condition.

Parameter	2-ph (20°)	2-ph (70°)	3-ph (20°)	3-ph (70°)	Unit
H_{PMmin}	921	888	932	881	kA/m
H_cJ_{min}	1592	1154	1592	1154	kA/m

As can be seen from Table 13, minimum coercive force values are significantly higher than the demagnetization field strengths. Estimated demagnetization temperature during worst short circuit condition is 103.4 °C, which is well above the estimated operating temperature. Conducted short circuit simulations are truly worst-case scenarios and should not occur in real life under any circumstances. In these simulations, the entire machine is short circuited at machine terminals, thus neglecting the effect of cables between machine and converters. As the machine design is segmented and driven with multiple frequency converters, such

situation will not occur, but rather smaller part of the machine would be short circuited under fault.

4.4.2 Unbalanced Magnetic Pull

Unbalanced magnetic pull (UMP) is a linear radial magnetic force. It can occur in permanent magnet machines for two reasons. First is non symmetrical winding distribution when all winding loops of the same phase are placed on the same side of the machine. This can be avoided by using suitable winding topologies, which themselves do not produce UMP. Second reason is rotor eccentricity, which can be caused by misalignment, insufficient rotor supporting by the bearings or flexible rotor or stator structure. Large values of UMP effects on bearing loads and reduces their lifetime if not thoroughly considered during design phase.

Simulation of UMP requires modelling of the entire machine geometry. Model does not need windings since used winding does not create unbalanced magnetic pull. Stator core, airgap region, permanent magnets and rotor must be modelled. Force created by the maximum eccentricity of 4 mm is illustrated in Figure 24.

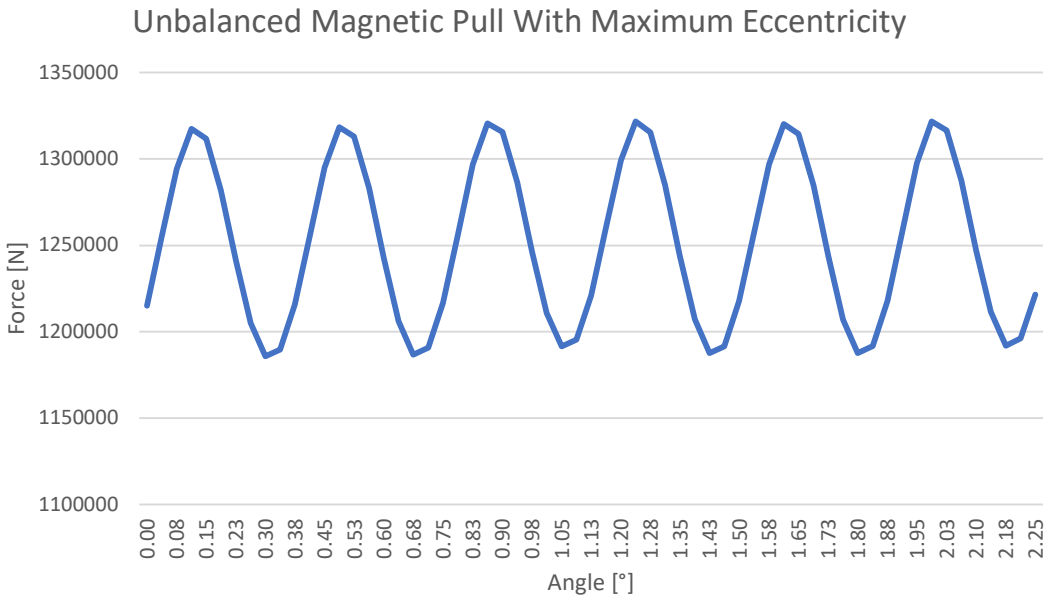

Figure 24. Unbalanced magnetic pull with maximum eccentricity of 4 mm.

Unbalanced magnetic pull mean value is 1251.80 kN with the eccentricity of 4 mm. This gives a spring constant of 312.95 kN/mm for UMP. This value should be used during mechanical design of frame, bearing and other supportive structures.

5 Conclusions and Discussion

As the result of this thesis, 28 MW machine design with permanent magnet modules was prepared. Electromagnetic performance meets previously set boundary conditions and efficiency is clearly higher than in typical electrically excited synchronous machines.

Thesis boundaries were set to electromagnetic design of the high torque low rotational speed permanent magnet machine. These consisted of winding design, geometrical design of stator lamination stack, permanent magnets, and rotor lamination pack for fractional slot machine. Existing topology of The Switch's permanent magnet module for the final design of the machine was used. Topology used was shown to fit this purpose and be mechanically robust and efficient. Previously developed manufacturing and mounting methods also contributed to the choice.

Rigidness of the rotor and the stator stack assembled to the frame must be evaluated with mechanical finite element analysis before prototype of the machine is manufactured to ensure that maximum eccentricity of 4 mm can be achieved. If it is found that structure is not rigid enough to withstand the forces created to the stator by unbalanced magnetic pull of the rotor magnets during eccentricity, design must be evaluated again. Fortunately, electromagnetic performance does not usually suffer when adding rigidity with more material.

Machine design voltage level of 690 V was selected as the insulation system of such machine is well known. Voltage level choice has no significant or adverse effect on used structure or design. The current of the machine is high and if this is found to be not feasible because of supply cabling or inverter size, in further studies, design can be made with medium voltage level by adjusting winding parameters and insulations. With advancements in permanent magnet materials and their properties, fractional slot concentrated wound machine type should be evaluated again. If acceptable level of losses in permanent magnets and rotor yoke would be possible, this winding type would decrease losses further and even better efficiency could be achieved.

References

Deeb, R. 2011. Calculation of Eddy Current Losses in Permanent Magnets of Servo Machine. Department of Power Electrical and Electronic Engineering, Faculty of Electrical Engineering and Communication, pp. 5.

Gavrila, H., (Paltanea), V.M., Paltanea, G., Scutaru, G. & Peter, I. 2017. New Trends in Energy Efficient Electrical Machines. Procedia Engineering, 181, pp. 568–574. URL: https://doi.org/10.1016/j.proeng.2017.02.435.

Kana Padinharu, D.K., Li, G.J., Zhu, Z.Q., Azar, Z., Clark, R. & Thomas, A. 2020. Effect of Airgap Length on Electromagnetic Performance of Surface Mounted Permanent Magnet Vemier Machine. URL: https://doi.org/10.1109/ICEM49940.2020.9270829. Accessed: 9 May 2023.

Kurronen, P. 2003. Torque vibration model of axial-flux surface-mounted permanent magnet synchronous machine. Dissertation. Lappeenranta University of Technology. URL: https://lutpub.lut.fi/handle/10024/31177. Accessed: 12 October 2023.

Pyrhonen, J., Jokinen, T. & Hrabovcová, V. 2014. Design of rotating electrical machines. Wiley. Chichester, West Sussex, United Kingdom.

Rilla, M. 2012. Design of salient pole PM synchronous machines for a vehicle traction application – Analysis and. Dissertation. Lappeenranta University of Technology. URL: https://lutpub.lut.fi/handle/10024/86335. Accessed: 11 October 2023.

Rosu, M., Saitz, J. & Arkkio, A. 2005. Hysteresis model for finite-element analysis of permanent-magnet demagnetization in a large synchronous machine under a fault condition. IEEE Transactions on Magnetics, 41, 6, pp. 2118–2123. URL: https://doi.org/10.1109/TMAG.2005.848319.

Ruuskanen, V. 2011. Design Aspects of Megawatt-Range Direct-Driven Permanent Magnet Wind Generators. Dissertation. Lappeenranta University of Technology. Lappeenranta. URL: https://lutpub.lut.fi/handle/10024/72627. Accessed: 9 May 2023.

Salminen, P. 2004. Fractional slot permanent magnet synchronous machines for low speed applications. Dissertation. Lappeenranta University of Technology. URL: https://lutpub.lut.fi/handle/10024/31164. Accessed: 8 August 2023.

Suuronen, O. 2019. Permanent Magnet Rotor Optimization. Masters Thesis. Lappeenranta University of Technology. Lappeenranta. URL: http://lutpub.lut.fi/handle/10024/159725. Accessed: 19 September 2023.

The Switch Engineering Oy, 2023a, Guidelines for PMM, Internal document.

The Switch Engineering Oy, 2021, Market Study High-torque, low-speed electrical machines, Internal document.

The Switch Engineering Oy, 2023b, Permanent magnet material info, Internal document.